ADVANCED PHOTONICS RESEARCH
Open Access
www.adpr-journal.com

Single-Step Tabletop Fabrication for Low-Attenuation Terahertz Special Optical Fibers

Md. Saiful Islam, Jakeya Sultana, Jonas H. Osório, Alex Dinovitser, Brian W-H. Ng, Fetah Benabid, Heike Ebendorff-Heidepriem, Derek Abbott, and Cristiano M. B. Cordeiro*

Amid the search for efficient terahertz transmission and gas sensing, all-polymer terahertz waveguides attract significant interest due to their compactness and capability for providing environmentally robust systems. The high loss within metals and dielectrics in the terahertz range makes it challenging to build a low loss, mechanically stable, and broadband terahertz waveguides. In this context, hollow waveguides made of Zeonex are promising for attaining low transmission loss in the terahertz range. Herein, a microstructured hollow hexagonal-core fiber (HCF) is investigated, which exhibits low loss, near-zero dispersion, wide operating bandwidth, and is suitable as a gas sensor. Notably, HCF fabrication is carried out by exploiting an efficient single-step extrusion method—by a standard filament extruder and a puller; hence the production cost is low compared with conventional extrusion methods. This introduces a novel way of fabricating complex and low-loss terahertz fibers. The experiments demonstrate that an HCF can achieve remarkably low attenuation and near-zero flattened dispersion as compared with any other terahertz fibers. The resulting HCFs are easy to handle and have high thermal and chemical stability. These results bring significant advancements for terahertz fiber fabrication, low-loss ultrafast short-distance terahertz transmission, and sensing in the terahertz spectral domain.

1. Introduction

The new frontier in terahertz research contains a significant number of cutting-edge applications, including label-free and noninvasive molecular detection, DNA hybridization probing, pharmaceutical drug testing, and high-speed short-range optical communications.[1–6] Terahertz technology also has significant potential for biomedical spectroscopy applications due to its ability to probe molecular interactions.[7–16] Moreover, it can be potentially applied to security screening as it can penetrate plastics, cardboard, and leather.[17] This motivates the interest in advancing terahertz technology as the demand for state-of-the-art terahertz sources, detectors, and waveguides is growing.

Although free-space terahertz propagation has been widely explored, terahertz transmission is profoundly affected by the water vapor present in the atmosphere. Transmission through waveguides is a promising approach, but the low transparency of materials is a significant challenge. Metal waveguides have been primarily considered, but their finite conductivity, inflexibility, and the surface roughness of metals limit their applicability.[18] To address this issue, the use of dielectric waveguides has gained attention, and encouraging results have been demonstrated. Polymers, such as Topas, Zeonex, Teflon, polymethylpentene (TPX), and HDPE, have emerged as materials of interest as they present a lower absorption coefficient than other dielectrics and glasses.[19]

In this context, the use of microstructured optical fibers (MOFs) emerges as an efficient approach for obtaining waveguides with adequate loss, birefringence, and dispersion levels. Indeed, the use of MOFs for the terahertz range is a growing trend.[20–33] Porous-core fibers, for example, have holes within

M. S. Islam, J. Sultana, A. Dinovitser, B. W. H. Ng, D. Abbott
School of Electrical & Electronic Engineering
University of Adelaide
Adelaide, SA 5005, Australia
E-mail: mdsaiful.islam@adelaide.edu.au

The ORCID identification number(s) for the author(s) of this article can be found under https://doi.org/10.1002/adpr.202100165.

DOI: 10.1002/adpr.202100165

M. S. Islam, H. Ebendorff-Heidepriem, C. M. B. Cordeiro
Institute of Photonics and Advanced Sensing
University of Adelaide
Adelaide, SA 5005, Australia

J. H. Osório, F. Benabid
GPPMM group
XLIM Institute
CNRS UMR 7252
University of Limoges
Limoges 87060, France

C. M. B. Cordeiro
Institute of Physics 'Gleb Wataghin'
State University of Campinas
Unicamp
Campinas 13083–859, Brazil

the core region, which lessen the overlap between the optical mode and the waveguide material, allowing a reduction loss levels in the terahertz range.[5,34–45] However, despite all the endeavors toward the development of terahertz fibers with solid or porous cores, achieving low loss, low dispersion, broadband transmission, and ease of fabrication remain critical issues.

Hollow-core (HC) fibers, otherwise, arise as the most appropriate choice for attaining optimum terahertz beam transmission. It is because, in HC fibers, the modes propagate through a hollow channel with low interaction with the fiber material. HC fibers can guide light either under photonic bandgap (PBG)[46] or inhibited coupling (IC)[47] mechanisms. In PBG fibers, mode guidance is possible because the cladding microstructure is such that there are no photonic states, within a specific frequency range, to which the core mode can be coupled. By contrast, in IC fibers, the core and cladding modes coexist. Low loss propagation is then achieved by minimizing the coupling between core and cladding modes. This coupling inhibition is attained by reducing the spatial overlap between the modes and by obtaining a strong mismatch between their transverse phases.[48,49]

Indeed, the excellent performance of IC fiber designs (e.g., kagome,[50,51] tubular,[48,49] conjoined-tubes,[52] nested-tubes,[53] and hybrid kagome–tubular[54] lattice designs) operating in the visible and infrared spectral ranges have been recently demonstrated in the literature. However, although terahertz HC fibers have been assessed in simulation studies, there are very few reports on experimental results regarding the operation of those fibers in the terahertz range.[55] In this context, it is noteworthy that 3D printing technology has appeared as a potentially useful technique for fabricating terahertz fibers.[30,56,57]

One reason is the larger dimensions of MOFs needed for guiding terahertz, compared with MOFs for the visible and IR ranges. The larger dimensions allow direct 3D printing or extrusion of the fiber itself, which is not possible for MOFs in the visible–IR range, where only the preform can be printed and a draw process is necessary to achieve the small dimensions. Also, terahertz fibers have shorter lengths compared with visible-IR fibers, which also make terahertz fibers more suited for simple fabrication techniques such as 3D printing.

In this study, we investigate a special HC terahertz fiber fabricated using Zeonex and a direct manufacturing technique based on a horizontal extruder. In addition to its low loss in the terahertz range, Zeonex presents high thermal and chemical stability and low water absorption. The fiber geometry has a hexagonal-shaped HC, which is connected to the outer jacket via six radial struts. The fabrication method uses a recently developed single-step technique,[58] which is here extended to fabricate a terahertz waveguide for the first time. We report the fabrication of fibers with different dimensions, as well as the characterization and simulation of their loss, dispersion, and gas sensing properties. The results reported herein will potentially contribute to the development of low-loss ultrafast short-distance terahertz transmission and ultrasensitive gas sensing measurements. Moreover, our manufactured fiber and other fibers manufactured in a similar fashion can potentially be used for lab-in-fiber devices for terahertz signals.[59]

2. Fiber Design and Fabrication

Figure 1a shows the fiber design we explore herein. It consists of a hollow hexagonal-core fiber (HCF), with Zeonex as the bulk material. In the fiber structure, six radial struts connect the hexagonal core contour to the outer jacket. Here, we denote the core side length as S_1 and its thickness as t. The radial struts have a length of S_2. The fiber microstructure is inscribed in a circle with a diameter $D_{\text{int}} = 2(S_1 + S_2)$, and the outer diameter of the fiber is defined as $D_{\text{ext}} = D_{\text{int}} + 2J$, where J is the outer jacket thickness. Previous studies have used similar fiber designs aiming at light transmission through ultraviolet, visible, and infrared wavelengths,[60–62] and the realization of sensing experiments.[63]

The advantage of such a standard waveguide structure is its straightforward fabrication procedure, which only requires a tabletop extruder.[58] In this structure, terahertz waves propagate through the fiber core due to the IC guidance mechanism.[47] It allows low loss transmission bands where the core mode coupling to the cladding modes is minimized. The coupling between core and cladding modes can be assessed in the light of coupled-mode theory, which provides the conditions for achieving low

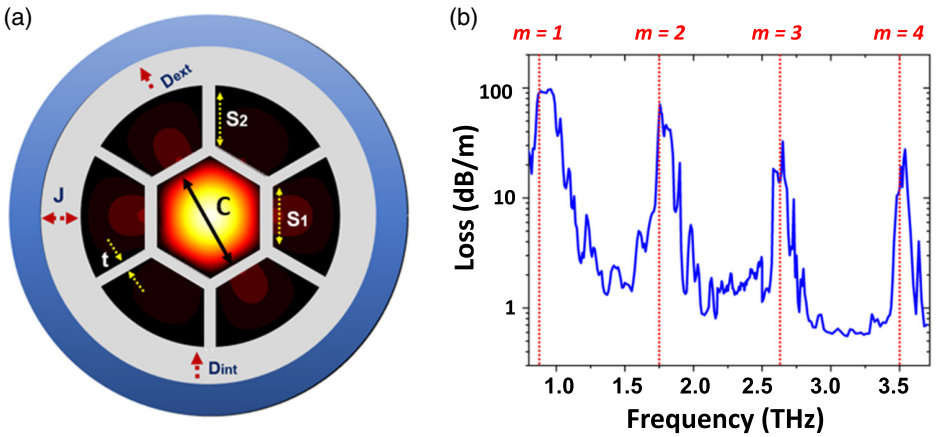

Figure 1. a) Cross-sectional schematic of the proposed hollow HCF, where the external blue region indicates the perfectly matched layer (PML) boundary condition. b) Typical simulated loss spectrum (using $S_1 = 1200\ \mu\text{m}$, $S_2 = 1170.6\ \mu\text{m}$, $t = 148\ \mu\text{m}$, and $J = 700\ \mu\text{m}$).

loss guidance through the fiber core. For example, it allows optimum guidance through the core that can be attained by reducing the overlap between the core and cladding modes fields and by attaining a strong mismatch between the core and cladding modes transverse phases.[47] The cladding modal spectrum of IC fibers is characterized by a quasicontinuum of modes.[47] This feature of the IC fiber modal spectrum is typically assessed by exploring the density of photonic states (DOPSs)[64] of the structure, which maps its cladding modes in the effective refractive index and frequency space.[47] The low-loss transmission bands are spectrally separated from each other by high-loss narrow bands. The latter is centered at high loss frequencies, f_{high}, given by Equation (1), and correspond to a resonant coupling between the core mode of interest with the cladding struts. Here, m is the resonance order, c is the speed of light, t is the cladding strut thickness, n_{clad} is the cladding refractive index, and n_{core} is the core refractive index.[48,49,65] Figure 1b shows a typical loss spectrum of such a structure, which is simulated by using a finite element method-based mode solver, COMSOL Multiphysics. In Figure 1b, the fiber parameters are $S_1 = 1200\,\mu\text{m}$, $S_2 = 1170.6\,\mu\text{m}$, $t = 148\,\mu\text{m}$, and $J = 700\,\mu\text{m}$, similar to one of our fabricated fibers. The Zeonex refractive index is set to $n = 1.529$ and its absorption coefficient to $\alpha = 0.2\,\text{cm}^{-1}$, as recently measured for planar Zeonex samples.[19] Note that, the environmental loss that we experience during experiment is not considered in simulation. The high loss frequencies calculated by Equation (1) shown as dotted vertical lines in Figure 1b, and is given as follows

$$f_{\text{high}} = mc/\left[2t\sqrt{n_{\text{clad}}^2 - n_{\text{co}}^2}\right] \tag{1}$$

The fabrication of the proposed fiber is carried out using a tabletop horizontal extruder designed for producing 3D printer filaments (EX2 Filabot). Notably, this is the unique piece of equipment needed for producing the terahertz fiber, we describe in this article. The method for obtaining the fibers is shown in **Figure 2**a. The operation is based on feeding the extruder screw with polymer pellets via a top hopper, whereas a heating element increases the plastic temperature. A special nozzle (Figure 2b) is 3D printed in titanium[58] and designed to present an external cross section that defines a solid hexagon linked to an external hollow jacket by six hollow channels (Figure 2c, left). The air struts in the nozzle are 0.8 mm thick. The internal nozzle diameter measures 12 mm. The internal construction of the nozzle follows a previously developed concept.[66] It allows the nozzle to block the material flow through its exit face in the regions where the fiber holes are designed to be. The fiber that emerges from the nozzle has, therefore, solid struts and a HC (Figure 2c, right). During the fabrication, the extrusion screw rotation speed can be adjusted, and typical values correspond to a material feed rate between 0.05 and 0.1 g s^{-1}. In addition, the temperature is set to 220 °C, and the extruded material has an initial external diameter that matches the nozzle's internal diameter, i.e., 12 mm.

Table 1. Geometrical parameters of the fabricated fibers.

Fiber sample	Strut thickness, t [μm]	Core diameter, C [mm]	Fiber diameter, D_{ext} [mm]	Fiber length, L [mm]
#1	22 ± 5	0.6	2.0	90
#2	65 ± 10	1.6	6.5	40
#3	95 ± 10	2.0	7.3	20
#4	155 ± 10	2.2	8.0	45

As mentioned earlier, Zeonex, a cyclo-olefin polymer (COP), is chosen as the fiber material for its low water absorption, moldability,[65] favorable chemical resistance,[19] and low loss in the terahertz frequency range.[19,67,68] The combination of these properties places Zeonex favorably compared with Teflon, Topas, high density poly ethylene (HDPE), and polymethyl methacrylate (PMMA). In this method, all polymers that can be extruded including, but not limited, to all those used in filament 3D printers can also be used as fabrication materials.

Here, Zeonex 480R commercial pellets[69] (with a density of 1.01 g cm^{-3}, glass transition temperature of 138 °C, and water absorption smaller than 0.01%) are selected. In this work, we target thick fibers with core diameters between 1 and 2 mm, for operation in the 0.5–3.5 THz range. Here, the draw down ratio of the dimensions of the material emerging from the die exit to the final fiber is quite small (from 12 to 5–8 mm typically). To achieve such a small reduction in dimensions, the extruded material is manually pulled at a low rate (few mm s^{-1}). However, a special spool machine can be used in future to improve manufacturing repeatability. To demonstrate the potential of the technique for producing fibers with different parameters, we report on the fabrication of four fibers, whose geometrical dimensions are shown in **Table 1**. The error estimation in the strut thickness, t, is made by considering multiple measurements carried out under an optical microscope. Remarkably, such a straightforward fabrication technique can yield fibers with struts within a considerable thickness range, namely between 20 and 160 μm. This has been achieved by

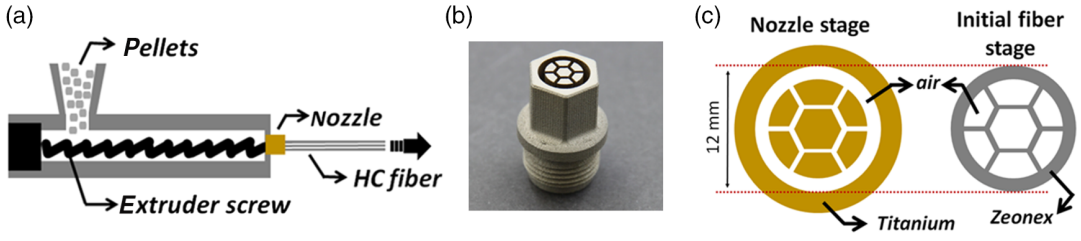

Figure 2. a) Lateral schematic view of the horizontal extruder showing the extruder screw, the feeding pellets hopper, specially designed nozzle, and the pulled terahertz HC fiber. b) Picture of the manufactured nozzle. c) Schematic top view of the nozzle and the fiber with the hexagonal-shaped core.

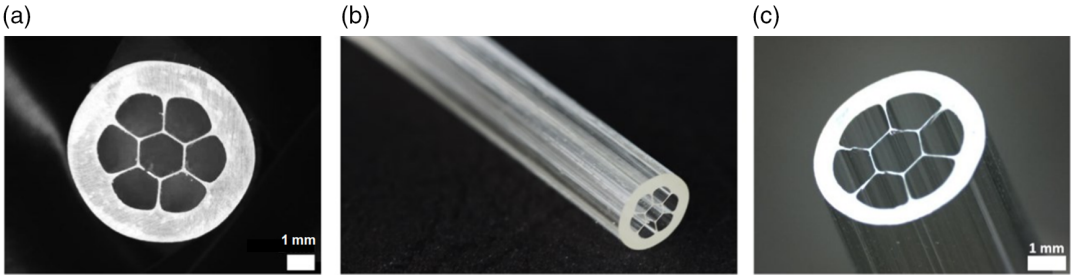

Figure 3. Representative images of the fabricated samples. a) Frontal and b) lateral views of fiber sample #3. c) Image of a fiber with an outer diameter of 4.4 mm, a core diameter of 1.2 mm, and struts thickness of 28 µm.

changing the draw rate, whereas the feed rate has been kept constant. **Figure 3** shows representative images of the fabricated fibers.

Recently, we researched 3D printed HC fiber, and we found that the surface of the 3D-printed fibers comes with a significant number of horizontal and vertical lines, hindering proper transmission in the terahertz domain. In comparison with 3D printing, our table-top fabrication method provides fibers with higher geometrical quality, fibers with thinner features along its cross section and samples with reduced surface roughness and lower losses.[70]

The main manufacturing parameters are the nozzle temperature, nozzle design, feed rate and pulling rate. We use a compact and ultralow-cost tabletop extruder to show that even this simple equipment can be used to produce high-quality samples. The fibers are manually pulled as the pulling rate is very low. To further improve the process, including the geometrical fiber repeatability, a special spool machine and a more advanced extruder (for compact tabletop operation) with precise temperature control along the extruder hot zone can potentially be used.

3. Fiber Characterization

3.1. Loss Measurement and Simulation

To characterize the fiber performance in the terahertz range, an Advantest TAS7400TS terahertz optical sampling system is used. The system is built with a dual-channel ultrashort pulse laser for free-space terahertz generation and detection.[71] In the experiment (shown in **Figure 4**), a gold-coated parabolic mirror with a focal length of 100 mm is used to focus the beam toward the waveguide core, and an iris is used to block undesired signals coupling to the core. The fiber waveguide is then placed on a translation stage, and a specially designed 3D-printed fiber holder is used to provide mechanical support. To ensure that the terahertz beam is coupled to the fiber core only, we wrap the waveguide with aluminum foil, while keeping the core region unblocked. The system is enclosed in a custom-made purge box filled with dry air, to minimize the presence of water vapor and avoid water-induced absorption. In addition, care is taken to ensure minimal humidity levels inside the purge box, via monitoring with a hygrometer. Typical reference and sample signals are shown in the inset in Figure 4.

The loss values of fiber samples #2 and #3 are estimated using the experimental setup shown in Figure 4. The reference (gray curve) and samples (blue and green curves) transmission spectra are presented on the left-hand side top graphs in **Figure 5**a,b. The shaded regions indicate the resonances of the microstructure struts, where the high loss occurs. These regions are calculated from Equation (1) by considering the strut thickness variations, as shown in Table 1. In the graphs on the right-hand side in Figure 5, we plot Equation (1) for $m = 1$ and $m = 2$ as a function of the fiber strut thickness to identify the expected high loss regions. The reference curves in Figure 5 have been obtained by directly shining the terahertz beam on the detector.

By considering the reference and sample spectra, one can calculate the transmission through the fiber sample, $T(\omega) = P_{\text{sam}}(\omega)/P_{\text{ref}}(\omega)$, where $P_{\text{ref}}(\omega)$ and $P_{\text{sam}}(\omega)$ are the reference and sample power spectra, respectively. Thus, one can estimate the total attenuation as $-10 \log T(\omega)$. The resulting values are shown in the bottom left-hand side plots in Figure 5 (left axis). As expected, low loss intervals are observed between the microstructure resonances. For fiber sample #2, the total attenuation figures are measured as 5.6 dB at 1.2 THz and 4.7 dB at 2.7 THz. For fiber sample #3, the total attenuation values are measured to be 9.2 dB at 0.95 THz, 6.2 dB at 2.2 THz, and 2.0 dB at 3.4 THz. The total attenuation of sample #4 is shown in **Figure 6**a. Sample #1, in contrast, could not be measured in

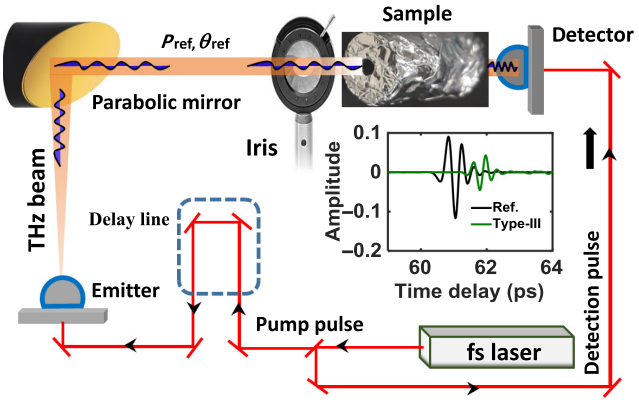

Figure 4. The experimental setup used to measure the fabricated fibers, which encompasses a femtosecond (fs) laser, a terahertz emitter, a detector, a parabolic mirror, an iris, and the sample itself. The whole system is enclosed in a purge box containing dry air. The inset shows typical reference and sampled signals.

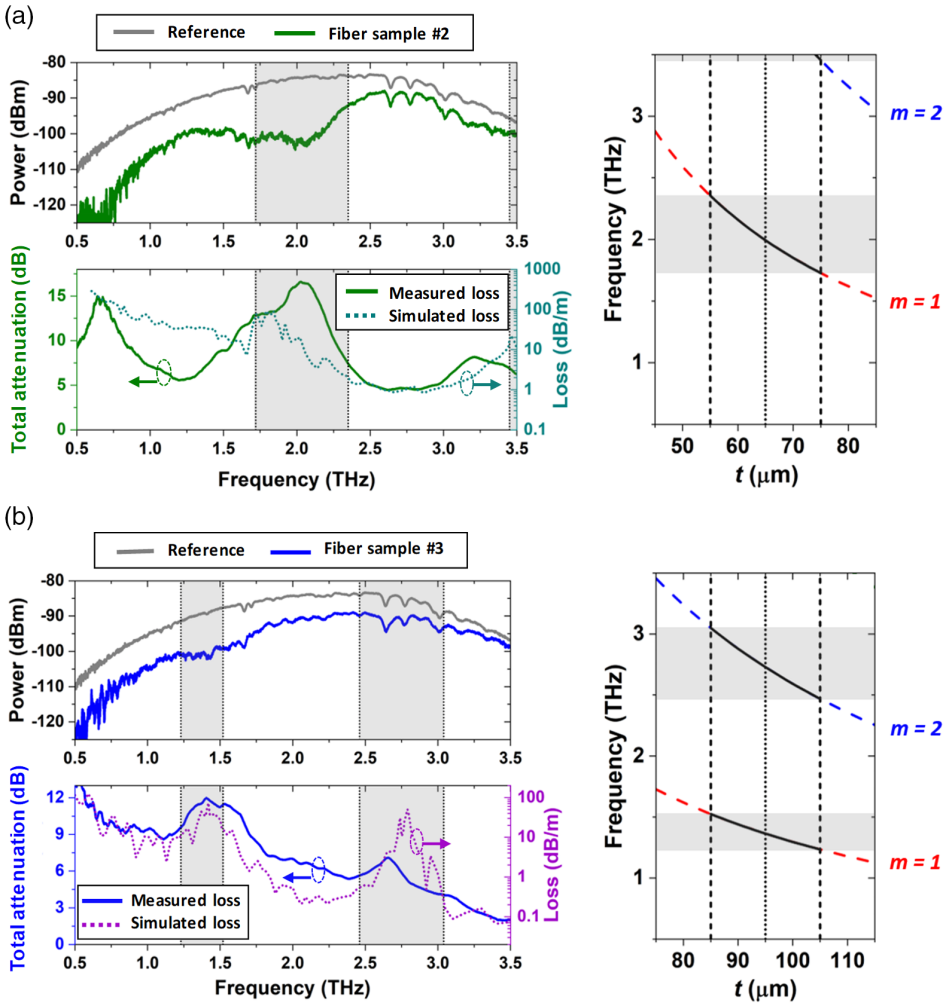

Figure 5. a) Left-hand side top: reference (gray curve) and fiber sample #2 (green curve) measured transmission spectra; left-hand side bottom: total attenuation (solid green curve) and simulated loss (dotted green curve). b) Left-hand side top: reference (gray curve) and fiber sample #3 (blue curve) measured transmission spectra; left-hand side bottom: total attenuation (solid blue curve) and simulated loss (dotted purple curve). Shaded regions indicate struts resonances, as shown in the plots presented on the right-hand side.

our system as its low-order resonances are expected to be around 5.9 and 11.8 THz.

In addition, numerical simulations using the finite element method (FEM) are carried out by considering the geometrical parameters of the fabricated fibers. The results are shown in Figure 5 as dotted green and dotted purple curves in the bottom left-hand side plots (right axis). As for the simulations in Figure 1b, the Zeonex refractive index is taken to be $n = 1.529$, and its absorption coefficient is set to $\alpha = 0.2\,\mathrm{cm}^{-1}$.[19] It is seen that minimum loss figures are calculated to be $33.7\,\mathrm{dB\,m}^{-1}$ at 1.2 THz and $0.95\,\mathrm{dB\,m}^{-1}$ at 2.7 THz for fiber sample #2. For fiber sample #3, loss values of $5.4\,\mathrm{dB\,m}^{-1}$ at 0.95 THz, $0.26\,\mathrm{dB\,m}^{-1}$ at 2.2 THz, and $0.07\,\mathrm{dB\,m}^{-1}$ at 3.4 THz are calculated.

The spectral locations of the resonances are reasonably well matched, between experimental and simulated results. One source of the discrepancies between measured and simulated data is assumed to be the existence of thickness variations in the struts that demark the core in the fabricated fibers. Further optimization of the fabrication process may reduce such imperfections, allowing to attain fibers with improved microstructures. Due to practical limitations in the current stage of the developed technique, we are unable to carry out cutback measurements using the fabricated samples. Thus, our analyses are restricted to the comparison between the total attenuation measured in the experiments (in dB, which includes coupling and transmission loss) and the simulated loss (in $\mathrm{dB\,m}^{-1}$, which accounts for confinement and absorption loss, hence not considering the coupling loss).

3.2. Dispersion and Sensing Measurements

The time-domain data obtained from the terahertz measurement system can be processed to account for the dispersion properties of the fibers. Thus, fast Fourier transforms (FFTs) can be applied to the obtained time-domain data to retrieve the magnitude and

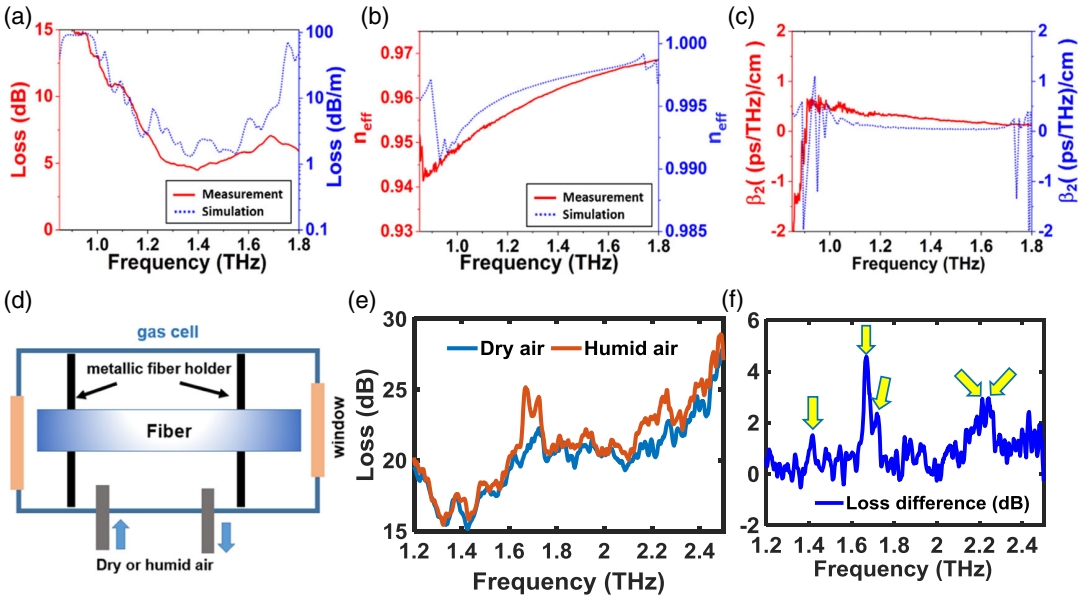

Figure 6. a) Experimental total attenuation (red curves) and simulated loss (dashed blue curves), b) effective refractive index, c) β_2 values for fiber sample #4, d) experimental setup for humid air sensing where a vacuum pump is used for continuous flow of humid air. During the measurements, the flow rate through the cell is kept significantly low. The cell contains a tissue wetted by milli-Q water. Two metallic discs are used to hold the fiber straight and block the stray of the terahertz signal coming from outside of the fiber, e) experimental loss measurement of a 45 mm long HC-THz fiber filled with dry and humid air from 1.2 to 2.4 THz. f) Loss difference between data in (e). Water absorption peaks are marked by arrows. Note, during the measurement, the air humidity is <5% in the external environment of the sensor setup, whereas it is >90% inside the gas cell.

phase in the frequency domain. In this process, the obtained phase is unwrapped between $-\pi$ and $+\pi$ to truncate unwanted noise above this range.[72] The effective refractive index, $n(\omega)$, can be obtained from Equation (2), where c is the speed of light, l is the fiber length, ω is the angular frequency, and $\Delta\phi(\omega)$ represents the phase difference between the reference and sample signals. In addition, the waveguide dispersion can be quantified from $n(\omega)$ as follows

$$n(\omega) = 1 + \left(\frac{c}{l}\right)\frac{\mathrm{d}\phi(\omega)}{\mathrm{d}\omega} \tag{2}$$

$$\beta_2 = \left(\frac{2}{c}\right)\frac{\mathrm{d}n(\omega)}{\mathrm{d}\omega} + \left(\frac{\omega}{c}\right)\frac{\mathrm{d}^2 n(\omega)}{\mathrm{d}\omega^2}\ \mathrm{ps/THz/cm} \tag{3}$$

Fiber sample #4 has been used in the dispersion measurements. The fiber loss and the frequency-dependent refractive index derived from the phase data in the terahertz measurements are shown in Figure 6a,b, respectively (red curves). In addition, the simulated loss and effective refractive index values are also shown in Figure 6a,b(dotted blue curves). In Figure 6b, one sees that experimental and simulated effective refractive index values are in close agreement. The measured values range from 0.948 to 0.967 in the frequency range between 1.0 and 1.7 THz. In contrast, the simulated ones range from 0.992 to 0.998 in the same frequency range. In addition, Figure 6c shows the experimental and simulation results for β_2 in fiber sample #4. The obtained β_2 values are remarkably low and flat (values between 0.12 and 0.60 (ps/THz)/cm between 1.0 and 1.7 THz) as compared with other experimentally reported low dispersion waveguides.[22,55,73–77]

The gas sensing capability of the proposed hollow fiber is verified using a water vapor detection measurement. Here, it is worth mentioning that water vapor has received major attention due to its abundance in the atmosphere and as a common absorber for terahertz electromagnetic waves. The undesirable vapor absorption lines are often referred to as a common impurity in spectroscopic studies. Therefore, water vapor in the atmosphere is one of the most suitable samples in testing the accuracy of a terahertz time-domain spectroscopy (THz-TDS) system.[78] Also, the rotational absorption characterization of water vapor is of interest in astronomical and atmospheric measurements.[79] The absorption peaks of water and hot water vapor,[80] for example, have been measured in different frequency ranges via the use of large gas cells.[78,81,82] In addition, small amounts of gas in a sealed fiber have been successfully detected using short and long length fibers.[83,84] However, there are very few studies for water vapor detection using terahertz fibers.[85]

Figure 6d shows the experimental setup used in such measurements. The HC fiber is inserted in a gas cell, composed of a plastic jar and two windows, whose atmospheric conditions can be controlled (via the use of a continuous supply of humid air, a flow of nitrogen, and an evacuation system). The air gap between each fiber end and the window is 3 mm and the fiber used in the experiments is 45 mm long. In turn, the gas cell length is 51 mm. The experimental procedure involves measuring the fiber transmittance between 1.2 and 2.4 THz when the fiber is filled with dry nitrogen and when the fiber is filled with humid air at room temperature.

In the measurements, sample #4 is placed on a metallic holder inside the gas cell and the transmitted signal is measured when

the fiber is in a dry environment and when water vapor is inserted in the gas cell. Figure 6e shows the loss of sample #4 when in dry and humid environments. It is seen that the loss is higher for the humid environment, as expected. Moreover, Figure 6f shows the difference between the curves in Figure 6d. This procedure allows clear identification of the absorption lines at 1.417, 1.669, 1.719, 2.213, and 2.265 THz, similarly to what has been achieved by Xin et al. and Cuia et al.[85,86] The absorption peaks are due to the vibrational and rotational transitions of the water vapor cluster bond. The absorption lines indicate the presence of water inside the fiber and demonstrates the potential of the fiber reported herein to act as a waveguide-based gas sensor.

4. Discussion

In this article, we report the design, fabrication, and characterization of low-cost HC fibers demonstrating low loss and near-zero dispersion in the terahertz range, which represents a promising path toward the accomplishment of efficient, low-loss, low-dispersion, and broadband terahertz transmission. A novel single-step fabrication method is adopted to provide efficient, simple, and low-cost fibers with different dimensions. The table-top fabrication method creates a new path for terahertz fiber fabrication and further research on terahertz transmission and sensing. The experimental analyses demonstrate fibers with total attenuation, transmission, and coupling loss of a few decibels in the studied frequency range, reaching values as low as 2 dB at 3.4 THz for sample #3 (20 mm long). Also, fibers with a near-zero dispersion of less than 0.6 ps/THz/cm are demonstrated. The results reported herein reveal the potential of such a remarkably simple fabrication technique for obtaining microstructured terahertz HC optical fibers.

While attaining low dispersion values is essential for adequately transmitting signals stemming from pulsed terahertz sources, having a low-loss hollow terahertz waveguide provides a promising path for the realization of ultrasensitive gas sensing. We anticipate that the analyses presented in this article will impact the development of low-loss ultrafast short-distance terahertz transmission devices and future gas sensing experiments. Finally, as the guidance in IC fibers is favored when the spatial overlap between the core mode and the modes in the cladding is minimized, designing fibers with hypocycloid-shaped core contours (i.e., negative curvature)[87,88] appears as an efficient approach for reducing the overlap between the core and cladding modes and, hence, for attaining fibers with lower loss levels. Thus, future developments can consider the fabrication of hypocycloid-shaped core fibers.

A future research direction can consider the actual contribution of water condensation inside the fiber and water vapor overlapping the air-guided modal profile.

Acknowledgements

This work was partially supported by the São Paulo Research Foundation (FAPESP) under grant 2018/10409-7. The authors thank Alson Ng, Evan Johnson, and Lijesh Thomas for their technical support. This work was supported by the ARC Centre of Excellence for Nanoscale BioPhotonics (CE14010003) and ARC LIEF Project (LE190100124). This work was carried out, in part, at the Optofab node of the Australian National Fabrication Facility (ANFF), utilizing Commonwealth and South Australian State Government funding.

Conflict of Interest

The authors declare no conflict of interest.

Author Contributions

M.S.I.: conceived the idea, design, simulation, experiment, and manuscript preparation; J.S.: contributed to the simulation; J.H.O. and F.B.: contributed to writing, analysing the results, and reviewing; A.D.: contributed to experimentation; C.M.B.C.: conceived the idea and contributed to fabrication, signal processing, writing; H.E.H., B.W.-H.N., D.A., and C.M.B.C.: contributed to supervising the work, analysis, and checking the results. All authors proof-read the manuscript.

Data Availability Statement

Research data are not shared.

Keywords

gas sensors, hollow core fibers, low attenuation, tabletop fabrications, terahertz fibers

Received: June 14, 2021
Revised: September 2, 2021
Published online: October 10, 2021

[1] G. Gallot, S. P. Jamison, R. W. McGowan, D. Grischkowsky, *J. Opt. Soc. Am. B* **2000**, *17*, 851.
[2] S. Atakaramians, V. S. Afshar, T. M. Monro, D. Abbott, *Adv. Opt. Photonics* **2013**, *5*, 169.
[3] P. H. Siegel, *IEEE Trans. Microwave Theory Tech.* **2004**, *52*, 2438.
[4] M. S. Islam, J. Sultana, A. Dinovitser, B. W.-H. Ng, D. Abbott, *Opt. Mater.* **2018**, *79*, 336.
[5] M. S. Islam, S. Rana, M. R. Islam, M. Faisal, H. Rahman, J. Sultana, *IET Commun.* **2016**, *10*, 2179.
[6] M. S. Islam, J. Sultana, A. Dinovitser, M. Faisal, M. R. Islam, B. W.-H. Ng, D. Abbott, *Appl. Opt.* **2018**, *57*, 666.
[7] J. Sultana, M. S. Islam, D. Abbott, *Electron. Lett.* **2018**, *54*, 61.
[8] D. M. Mittleman, R. H. Jacobsen, R. Neelamani, R. G. Baraniuk, M. C. Nuss, *Appl. Phys. B* **1998**, *67*, 379.
[9] E. Gerecht, K. O. Douglass, D. F. Plusquellic, *Opt. Express* **2011**, *19*, 8973.
[10] H. Lin, W. Withayachumnankul, B. M. Fisher, S. P. Mickan, D. Abbott, *Proc. SPIE Terahertz Photonics* **2007**, *6840*, 68400X.
[11] E. Pickwell, V. P. Wallace, *J. Phys. D: Appl. Phys.* **2006**, *39*, R301.
[12] M. S. Islam, J. Sultana, K. Ahmed, A. Dinovitser, M. R. Islam, B. W.-H. Ng, D. Abbott, *IEEE Sens. J.* **2018**, *18*, 575.
[13] M. S. Islam, J. Sultana, M. Biabanifard, M. J. Nine, Z. Vafapour, A. Dinovitser, C. M. B. Cordeiro, B. W.-H. Ng, D. Abbott, *Carbon* **2020**, *158*, 559.
[14] M. S. Islam, J. Sultana, A. A. Rifat, A. Dinovitser, B. W.-H. Ng, D. Abbott, *IEEE Sens. J.* **2018**, *18*, 4073.
[15] B. S. Williams, *Nat. Photonics* **2007**, *1*, 517.

[16] W. L. Chan, J. Deibel, D. M. Mittleman, *Rep. Prog. Phys.* **2007**, *70*, 1325.
[17] G. E. Tsydynzhapov, P. A. Gusikhin, V. M. Muravev, I. V. Andreev, I. V. Kukushkin, *43rd Int. Conf. on Infrared, Millimeter, and Terahertz Waves (IRMMW-THz)*, Nagoya, Japan, September 2018.
[18] T. Jeon, J. Zhangm, D. Grichkowsky, *Appl. Phys. Lett.* **2005**, *86*, 161904.
[19] M. S. Islam, J. Sultana, C. M. B. Cordeiro, A. L. S. Cruz, A. Dinovitser, B. W.-H. Ng, D. Abbott, *44th Int. Conf. on Infrared, Millimeter, and Terahertz Waves (IRMMW-THz)*, Paris, France, September 2019.
[20] Md. S. Islam, C. M. B. Cordeiro, M. A. R. Franco, J. Sultana, A. L. S. Cruz, D. Abbott, *Opt. Express* **2020**, *28*, 16089.
[21] J. A. Harrington, R. George, P. Pedersen, *Opt. Express* **2004**, *12*, 5263.
[22] J. Anthony, R. Leonhardt, A. Argyros, *Opt. Express* **2013**, *21*, 2903.
[23] M. S. Vitiello, J.-H. Xu, M. Kumar, F. Beltram, A. Tredicucci, O. Mitrofanov, H. E. Beere, D. A. Ritchie, *Opt. Express* **2011**, *19*, 1122.
[24] C. Themistos, B. M. A. Rahman, M. Rajarajan, K. T. V. Grattan, B. Bowden, J. A. Harrington, *J. Lightwave Technol.* **2007**, *25*, 2456.
[25] B. Bowdem, J. A. Harrington, O. Mitrofanov, *Opt. Lett.* **2007**, *32*, 2945.
[26] B. Bowden, J. A. Harrington, O. Mitrofanov, *J. Appl. Phys. Lett.* **2008**, *93*, 181104.
[27] B. Bowden, J. A. Harrington, O. Mitrofanov, *J. Appl. Phys.* **2008**, *104*, 093110.
[28] Y. Matsuura, E. Takeda, *J. Opt. Soc. Am. B* **2008**, *25*, 1949.
[29] X.-L. Tang, Y.-W. Shi, Y. Matsuura, K. Iwai, M. Miyagi, *Opt. Lett.* **2009**, *34*, 2231.
[30] L. D. Van Putten, J. Gorecki, E. N. Fokoua, A. Apostolopoulos, F. Poletti, *Appl. Opt.* **2018**, *57*, 3953.
[31] A. Stefani, S. C. Fleming, B. T. Kuhlmey, *APL Photonics* **2018**, *3*, 051708.
[32] C.-H. Lai, B. You, J. Y. Lu, T. A. Liu, J.-L. Peng, C.-K. Sun, H.-C. Chang, *Opt. Express* **2009**, *18*, 309.
[33] H. Li, S. Atakaramians, R. Lwin, X. Tang, Z. Yu, A. Argyros, B. T. Kuhlmey, *Optica* **2016**, *3*, 941.
[34] M. S. Islam, J. Sultana, S. Rana, M. R. Islam, M. Faisal, S. F. Kaijage, D. Abbott, *Opt. Fiber Technol.* **2017**, *34*, 6.
[35] M. S. Islam, M. R. Islam, M. Faisal, A. S. M. S. Arefin, H. Rahman, J. Sultana, S. Rana, *Opt. Eng.* **2016**, *55*, 076117.
[36] M. S. Islam, J. Sultana, J. Atai, D. Abbott, S. Hana, M. R. Islam, *Appl. Opt.* **2017**, *56*, 1232.
[37] A. Markov, M. Skorobogatiy, *Opt. Express 21*, 12728.
[38] S. Atakaramians, S. Afshar, H. Ebendorff-Heidepriem, M. Nagel, B. M. Fischer, D. Abbott, T. M. Monro, *Opt. Express* **2009**, *17*, 14053.
[39] N. Chen, J. Liang, L.-Y. Ren, *Appl. Opt.* **2013**, *52*, 5297.
[40] A. Hassani, A. Depuis, M. Skorobogatiy, *Opt. Express* **2008**, *16*, 6340.
[41] A. L. S. Cruz, A. C. C. Migliano, M. A. R. Franco, *2013 SBMO/IEEE MTT-S Int. Microwave & Optoelectronics Conf. (IMOC)*, Rio de Janeiro, Brazil, August 2013.
[42] H. Bao, K. Nielsen, H. K. Resmussen, P. U. Jepsen, O. Bang, *Opt. Express* **2012**, *20*, 29507.
[43] S. F. Kaijage, Z. Ouyang, X. Jin, *IEEE Photonics Technol. Lett.* **2013**, *25*, 1454.
[44] K. Ahmed, S. Chowdhury, B. K. Paul, M. S. Islam, S. Sen, M. I. Islam, S. Asaduzzaman, *Appl. Opt.* **2017**, *56*, 3477.
[45] A. Aming, M. Uthman, R. Chitaree, W. Mohammed, B. M. Azizur Rahman, *J. Lightwave Technol.* **2016**, *34*, 5583.
[46] T. A. Birks, P. J. Roberts, P. S. J. Russell, D. M. Atkin, T. J. Shepherd, *Electron. Lett.* **1995**, *31*, 1941.
[47] F. Couny, F. Benabid, P. J. Roberts, P. S. Light, M. G. Raymer, *Science* **2007**, *318*, 1118.
[48] B. Debord, A. Amsanpally, M. Chafer, A. Baz, M. Maurel, J. M. Blondy, E. Hugonnot, F. Scol, L. Vincetti, F. Gérôme, F. Benabid, *Optica* **2017**, *4*, 209.
[49] B. Debord, F. Amrani, L. Vincetti, F. Gérôme, F. Benabid, *Fibers* **2019**, *7*, 16.
[50] M. Maurel, M. Chafer, A. Amsanpally, M. Adnan, F. Amrani, B. Debord, L. Vincetti, F. Gérôme, F. Benabid, *Opt. Lett.* **2018**, *43*, 1598.
[51] M. Chafer, J. H. Osório, F. Amrani, F. Delahaye, M. Maurel, B. Debord, F. Gérôme, F. Benabid, *IEEE Photonics Technol. Lett.* **2019**, *31*, 685.
[52] S. Gao, Y. Wang, W. Ding, D. Jiang, S. Gu, X. Zhang, P. Wang, *Nat. Commun.* **2018**, *9*, 2828.
[53] G. T. Jasion, T. D. Bradley, K. Harrington, H. Sakr, Y. Chen, E. N. Fokoua, I. A. Davidson, A. Taranta, J. R. Hayes, D. J. Richardson, F. Poletti, *Optical Fiber Communication Conf.*, paper Th4B.4, San Diego, California, United States, March 2020.
[54] F. Amrani, J. H. Osório, F. Delahaye, F. Giovanardi, L. Vincetti, B. Debord, F. Gérôme, F. Benabid, *Light Sci. Appl.* **2021**, *10*, 7.
[55] J. Anthony, R. Leonhardt, S. G. Leon-Saval, A. Argyros, *Opt. Express* **2011**, *19*, 18470.
[56] S. Yang, X. Sheng, G. Zhao, Y. Wang, Y. Yu, *J. Infrared, Millimeter, Terahertz Waves* **2019**, *40*, 720.
[57] A. L. S. Cruz, C. M. B. Cordeiro, M. A. R. Franco, *Fibers* **2018**, *6*, 43.
[58] C. M. B. Cordeiro, A. K. L. Ng, H. Ebendorff-Heidepriem, *Sci. Rep.* **2020**, *10*, 9678.
[59] S. Pissadakis, *Microelectronic Eng.* **2019**, *217*, 1111105.
[60] F. Gérôme, R. Jamier, J.-L. Auguste, G. Humbert, J.-M. Blondy, *Opt. Lett.* **2010**, *35*, 1157.
[61] J. R. Hayes, F. Poletti, M. S. Abokhamis, N. V. Wheeler, N. K. Baddela, D. J. Richardson, *Opt. Express* **2015**, *23*, 1289.
[62] A. Hartung, J. Kobelke, A. Schwuchow, J. Bierlich, M. A. Schmidt, T. Frosch, *Opt. Lett.* **2015**, *40*, 3432.
[63] G. Tsiminis, K. J. Rowland, E. P. Schartner, N. A. Spooner, T. M. Monro, H. Eberndorff-Heidepriem, *Opt. Express* **2013**, *24*, 5911.
[64] J. M. Pottage, D. M. Bird, T. D. Hedley, T. A. Birks, J. C. Knight, P. St. J. Russell, P. J. Roberts, *Opt. Express* **2003**, *11*, 2854.
[65] V. Setti, L. Vincetti, A. Argyros, *Opt. Express* **2013**, *21*, 3388.
[66] H. Ebendorff-Heidepriem, T. M. Monro, *Opt. Express* **2007**, *15*, 15086.
[67] G. Woyessa, A. Fasano, C. Markos, A. Stefani, H. K. Rasmussen, O. Bang, *Opt. Mater. Express*, **2017**, *7*, 286.
[68] J. Anthony, R. Leonhardt, A. Argyros, M. C. J. Large, *J. Opt. Soc. Am. B* **2011**, *28*, 1013.
[69] *Product Data Sheet (Zeonex 480R)*, **2015**.
[70] J. Sultana, M. S. Islam, C. M. B. Cordeiro, M. S. Habib, A. Dinovitser, M. Kaushik, B. W.-H. Ng, H. E. Heidepriem, D. Abbott, *IEEE Trans. Terahertz Sci. Technol.* **2021**, *11*, 245.
[71] *Advantest Corporation*, https://www.advantest.com/products/terahertzspectroscopic-imaging-systems (accessed: October 2019).
[72] P. U. Jepsen, *J. Infrared, Millimeter, Terahertz Waves* **2019**, *40*, 395.
[73] M. Mboyne, R. Mendis, D. M. Muttlemana, *Appl. Phys. Lett.* **2009**, *95*, 233506.
[74] R. Mendis, D. Grischkowsky, *Opt. Lett.* **2001**, *26*, 846.
[75] K. Wang, D. M. Mittleman, *Nature* **2004**, *432*, 376.
[76] H. Han, H. Park, M. Cho, J. Kim, *Appl. Phys. Lett.* **2002**, *80*, 2634.
[77] J. Anthony, R. Leonhardt, A. Argyros, M. C. J. Large, *J. Opt. Soc. Am. B.* **2002**, *28*, 5.
[78] M. V. Exter, Ch. Fattinger, D. Grischkowsky, *Opt. Lett.* **1989**, *14*, 1128.
[79] V. B. Podobedov, D. F. Plusquellic, K. E. Siegrist, G. T. Fraser, Q. Ma, R. H. Tipping, *J. Quant. Spectrosc. Radiat. Transfer* **2008**, *109*, 458.
[80] F. Matsushima, H. Odashima, T. Iwasaki, S. Tsunekawa, K. Takagi, *IEEE Trans. Instrum. Meas.* **1995**, *44*, 110.

[81] J. S. Melinger, Y. Yang, M. Mandehgar, D. Grischkowsky, *Opt. Express* **2012**, *20*, 6788.
[82] R. A. Cheville, D. Grischkowsky, *Opt. Lett.* **1998**, *23*, 531.
[83] B. You, J.-Y. Lu, C.-P. Yu, T.-A. Liu, J. Long, *Opt. Express* **2012**, *20*, 5858.
[84] T. Katagiri, T. Suzuki, Y. Matsuura, *Opt. Eng.* **2018**, *57*, 054104.
[85] X. Xin, H. Altan, A. Saint, D. Matten, R. R. Alfano, *J. Appl. Phys.* **2006**, *100*, 094905.
[86] H. Cuia, X. B. Zhang, J. F. Su, Y. X. Yang, Q. Fang, X. Y. Wei, *Optik* **2015**, *126*, 3533.
[87] Y. Y. Wang, N. V. Wheeler, F. Couny, P. J. Roberts, F. Benabid, *Opt. Lett.* **2011**, *36*, 669.
[88] B. Debord, M. Alharbi, T. Bradley, C. Fourcade-Dutin, Y. Y. Wang, L. Vincetti, F. Gérôme, F. Benabid, *Opt. Express* **2013**, *21*, 28597.